Automatic Surgical Reconstruction for Orbital Blow-Out Fracture via Symmetric Prior Anatomical Knowledge-Guided Adversarial Generative Network

Jiangchang Xu[1], Yining Wei[2], Huifang Zhou[2,4], Yinwei Li[2,4(✉)], and Xiaojun Chen[1,3(✉)]

[1] Institute of Biomedical Manufacturing and Life Quality Engineering, School of Mechanical Engineering, Shanghai Jiao Tong University, Shanghai, China
xiaojunchen@sjtu.edu.cn
[2] Department of Ophthalmology, Shanghai Ninth People's Hospital, Shanghai Jiao Tong University School of Medicine, Shanghai, China
dr_yinwei_li@foxmail.com
[3] Institute of Medical Robotics, Shanghai Jiao Tong University, Shanghai, China
[4] Shanghai Key Laboratory of Orbital Diseases and Ocular Oncology, Shanghai, China

Abstract. Orbital blow-out fracture (OBF) is a complex disease that can cause severe damage to the orbital wall. The ultimate means of treating this disease is orbital reconstruction surgery, where automatic reconstruction of the orbital wall is a crucial step. However, accurately reconstructing the orbital wall is a great challenge due to the collapse, damage, fracture, and deviation in OBF. Manual or semi-automatic reconstruction methods used in clinics also suffer from poor accuracy and low efficiency. Therefore, we propose a symmetric prior anatomical knowledge (SPAK)-guided generative adversarial network (GAN) for automatic reconstruction of the orbital wall in OBF. Above all, a spatial transformation-based SPAK generation method is proposed to generate prior anatomy that guides the reconstruction of the fractured orbital wall. Next, the generated SPAK is introduced into the GAN network, to guide the network towards automatic reconstruction of the fractured orbital wall. Additionally, a multi-function combination supervision strategy is proposed to further improve the network reconstruction performance. Our evaluation on the test set showed that the proposed network achieved a Dice similarity coefficient (DSC) of $92.35 \pm 2.13\%$ and a 95% Hausdorff distance of 0.59 ± 0.23 mm, which is significantly better than other networks. The proposed network is the first AI-based method to implement the automatic reconstruction of OBF, effectively

Supplementary Information The online version contains supplementary material available at https://doi.org/10.1007/978-3-031-43996-4_44.

H. Greenspan et al. (Eds.): MICCAI 2023, LNCS 14228, pp. 462–471, 2023.
https://doi.org/10.1007/978-3-031-43996-4_44

improving the reconstruction accuracy and efficiency of the fractured orbital wall. In the future, it has a promising application prospect in the surgical planning of OBF.

Keywords: Automatic surgery planning · Orbital blow-out fracture · Surgical reconstruction · Symmetric prior anatomical knowledge

1 Introduction

Orbital fractures represent a frequent occurrence of orbital trauma, with their incidence on the rise primarily attributed to assault, falls, and vehicle collisions [1]. Orbital blow-out fracture (OBF) is a frequent type of fracture where one of the orbital walls fractures due to external force, while the orbital margin remains intact [2]. It is a complex disease that can result in the destruction or collapse of the orbital wall, orbital herniation, invagination of the eyeball, and even visual dysfunction or changes in appearance in severe cases [3]. OBF repair surgery is the ultimate treatment for this disease and involves implanting artificial implants to repair and fill the fractured area. Automatic reconstruction of the orbital wall is a crucial step in this procedure to achieve precise preformed implants and assisted intraoperative navigation.

Orbital wall reconstruction is challenging due to the complex and diverse OBF types, as shown in Fig. 1, including (a) medial wall fracture, (b) floor wall fracture, (c) fractures in both the medial and floor walls, (d) roof wall fracture, (e) and other types. The orbital walls in these cases are often collapsed, damaged, fractured, deviated, or exhibit a large number of defects in severe cases, which makes reconstruction more difficult. Furthermore, the orbital medial and floor walls are thin bones with low CT gradient values and blurred boundaries, which further increases the complexity of reconstruction. Currently, commercial software is typically used for semi-automatic reconstruction in clinical practice. However, this method is inefficient and inaccurate, requiring tedious manual adjustment and correction. As a result, doctors urgently need fast and accurate automated surgical reconstruction methods.

Several automatic segmentation methods for the orbital wall have been explored in previous studies [4], such as Kim et al.'s [5] orbital wall modeling based on paranasal sinus segmentation and Lee et al.'s [6] segmentation algorithm of the orbital cortical bone and thin wall with a double U-Net network structure. However, they did not explore segmentation for OBF. Taghizadeh et al. [7] proposed an orbital wall segmentation method based on a statistical shape model and local template matching, but individualized differences and factors such as orbital wall deviation and collapse greatly affect its performance in fractured orbits. Deep learning-based algorithms for skull defect reconstruction have also been proposed, such as Li et al.'s [8] automatic repair network for skull defects, Xiao et al.'s [9] network model that estimates bone shape using normal facial photos and CT of craniomaxillofacial trauma, and Han et al.'s [10] craniomaxillofacial defect reconstruction algorithm with a statistical shape

model and individual features. However, these methods require the removal of the lesion area followed by reconstruction of the defect, which is different from OBF repair that directly performs orbital wall reconstruction without removal of the destroyed bone. The above methods may be less effective in cases of OBF where factors such as deviation, collapse, and fracture greatly impact the reconstruction network, reducing the reconstruction effect. As of now, there are no automated reconstruction methods reported for OBF surgery.

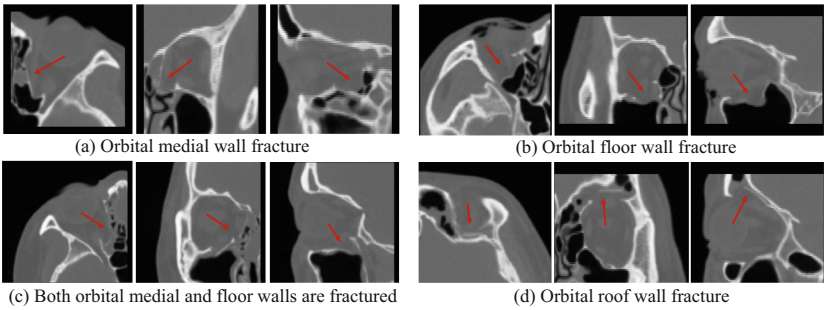

Fig. 1. Common types and reconstruction challenges of orbital blowout fractures.

To address the above challenges, this paper proposes a symmetric prior anatomical knowledge-guided adversarial generative network (GAN) for reconstructing orbital walls in OBF surgery. Firstly, the paper proposes an automatic generation method of symmetric prior anatomical knowledge (SPAK) based on spatial transformation, which considers that the symmetrical normal orbital anatomy can guide the reconstruction of the fractured orbital wall. Secondly, the obtained SPAK is used as a prior anatomical guidance for GAN to achieve more accurate automatic reconstruction of the orbital wall. To further improve the network's reconstruction performance, the paper adopts a supervision strategy of multi-loss function combination. Finally, experimental results demonstrate that the proposed network outperforms some state-of-the-art networks in fracture orbital wall reconstruction.

The main contributions of this paper are summarized as follows: (1) A GAN model guided by SPAK is developed for automatic reconstruction of the orbital wall in OBF surgery, which outperforms the existing methods. (2) The proposed method is the first AI-based automatic reconstruction method of the orbital wall in OBF surgery, which can enhance the repair effectiveness and shorten the surgical planning time.

2 Methods

The structure of the proposed SPAK-guided GAN is illustrated in Fig. 2, and it mainly comprises three components: automatic generation of SPAK, GAN network structure, and multiple loss function supervision. Each component is elaborated below.

2.1 Automatic Generation of SPAK Based on Spatial Transformation

The reconstruction of the orbital wall in OBF is a complex task, made more difficult when severe displacement or defects are present. However, since the left and right orbits are theoretically symmetrical structures, utilizing the normal orbital wall on the symmetrical side as prior anatomical guidance in the reconstruction network can aid in accuracy. Prior knowledge has been demonstrated to be effective in medical image computing [11–13]. Nonetheless, left and right orbits are not perfectly symmetrical, and the mirror plane can be challenging to locate, leading to substantial errors and unwieldy operations. To address these issues, we propose an automatic generation method for SPAK based on spatial transformations, as depicted in Fig. 2. The main steps of this method include: (1) obtaining the orbital ROI containing both orbits and resampling to ensure input image size consistency in the network; (2) using the sagittal plane as the central surface to separate the left and right orbits; (3) employing the 3D V-Net network to automatically segment the normal and fractured orbital walls, respectively, and acquire their respective segmentation results; (4) restoring the left and right orbital segmentation results to their original position to ensure spatial coordinate consistency; (5) mirror the orbital wall normally along the Y-axis plane, ensuring correspondence between the shape of the segmentation result from both the left and right orbital walls; (6) reconstructing the left and right orbital walls

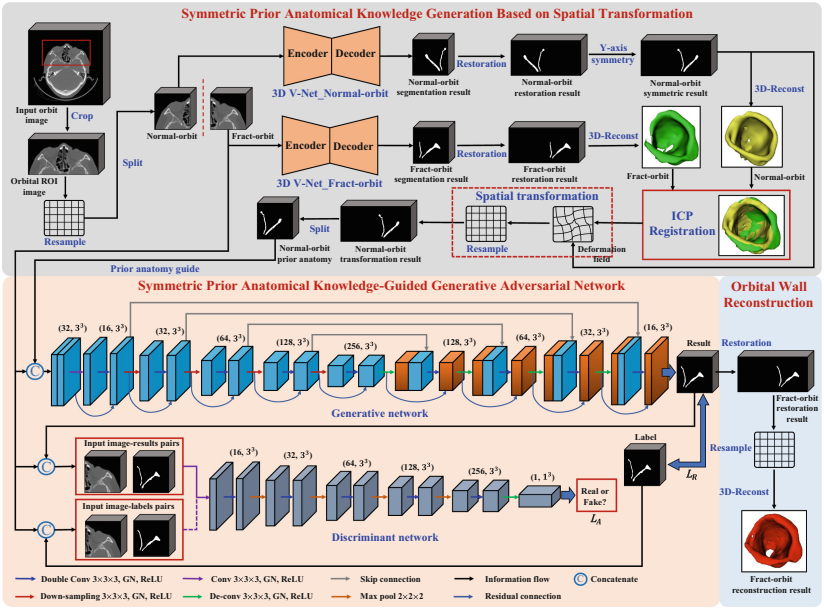

Fig. 2. Structure of the proposed symmetric prior anatomical knowledge-guided generative adversarial network for reconstructing the fractured orbital wall.

in 3D dimensions and obtaining their respective three-dimensional models; (7) using the ICP algorithm to register the normal and fractured orbital walls and acquire their deformation field; (8) based on the previous step, transforming the symmetrical normal orbital wall to the side of the fractured orbital wall using the deformation field; (9) separating the transformed normal orbital wall to obtain a single orbital wall that can serve as a SPAK to guide GAN.

2.2 SPAK-Guided GAN for Orbital Wall Reconstruction

Reconstructing the fractured orbital wall requires generative prediction of the damaged area, which is why we adopted the GAN. Our proposed SPAK-guided GAN consists of a generative network (GN) and a discriminative network (DN), as illustrated in Fig. 2. The GN uses a network structure based on 3D V-Net and consists of five encoded layers and four decoded layers to achieve automatic reconstruction of the fractured orbital wall. The input of the GN is the merged block of SPAK and the original image, which guides the GAN network to make more accurate predictions of the orbital wall. To expand the receptive field, each convolution layer uses two convolution stacks and includes residual connections to reduce gradient dissipation. The activation function is ReLU, and group normalization [14] is added after each convolution to prevent network overfitting. To avoid the loss of shallow features as the number of network layers increases, we added skip connections between the corresponding convolutional layers of the encoded and decoded sections. The DN identifies the authenticity of the reconstructed orbital wall and the ground truth to produce a more realistic orbital wall. It includes five encoded feature layers and one fully connected layer. Each encoded feature layer comprises stacked convolutions and a max-pooling layer with a filter kernel of $2 \times 2 \times 2$ and a step size of 2 to compress the feature map. The input of the DN is either the merged image block of the original image and the reconstructed orbital wall area or the original image and the ground truth. The DN distinguishes between the authenticity of these inputs. After restoring the output result of the network to the original position and resampling, we perform 3D reconstruction to obtain the reconstructed orbital wall model.

2.3 Multiple Loss Function Supervision for GAN

The GAN network's loss function comprises two components: the loss function of the discriminative network, denoted as $Loss_D$, and the loss function of the generative network, denoted as $Loss_G$. To enhance the reconstruction performance, we adopt a supervision strategy that combines multiple loss functions. To ensure that the GAN network can identify the authenticity of samples, we incorporate the commonly used discriminative loss function in GAN, as presented in Eq. (1).

$$Loss_D = \min_G \left[\max_D E_{x,y} \left[\log \left(D \left(x, y \right) \right) \right] + E_x \left[\log \left(1 - D \left(x, G \left(x \right) \right) \right) \right] \right], \quad (1)$$

where D represents the network discriminator, G represents the network generator, $G(x)$ represents reconstruction result, x represents input image, y represents ground truth.

To improve the accuracy of the reconstructed orbital wall, a combination of multiple loss functions is utilized in $Loss_G$. First, to better evaluate the area loss, the dice coefficient loss function $Loss_{dice}$ is adopted, which can calculate the loss between the reconstructed orbital wall region and the ground truth using Eq. (2). Secondly, due to the potential occurrence of boundary fractures and orbital wall holes during GAN reconstruction, the cross-entropy loss function $Loss_{ce}$ is added to $Loss_G$. Its equation is shown in (3) to evaluate the reconstruction of the boundary and holes.

$$Loss_{dice} = 1 - \frac{2\sum_i^N G\left(x_i\right) y_i}{\sum_i^N G\left(x_i\right)^2 + \sum_i^N {y_i}^2}, \tag{2}$$

$$Loss_{ce} = -\frac{1}{N}\sum_i^N \left[y_i log(G\left(x_i\right)) + \left(1 - y_i\right) log(1 - G\left(x_i\right))\right], \tag{3}$$

where N represents the total number of voxels, $G(x_i)$ represents the voxels of reconstruction results, y_i represents the voxels of ground truth.

Furthermore, an adversarial loss function L_{adv}, is also incorporated into $Loss_G$. This function evaluates the loss of the generator's output by the discriminator, thus enabling the network to improve its performance in reconstructing the fractured orbital wall. The equation for L_{adv} is shown in (4).

$$L_{adv} = \ E_x\left[\log\left(D\left(x, G\left(x\right)\right)\right)\right], \tag{4}$$

Finally, we combine the loss function $Loss_{dice}$, $Loss_{ce}$ and L_{adv} to obtain the final $Loss_G$, whose equation is shown in (5) and λ is the weight parameter.

$$Loss_G = Loss_{dice} + Loss_{ce} + \lambda \bullet L_{adv}. \tag{5}$$

3 Experiments and Results

3.1 Data Set and Settings

The dataset for this study was obtained from Shanghai Ninth People's Hospital Affiliated to Shanghai Jiao Tong University School of Medicine. It included 150 cases of OBF CT data: 100 for training and 50 for testing. Each case had a blowout orbital fracture on one side and a normal orbit on the other. For normal orbit segmentation training, 70 additional cases of normal orbit CT data were used. The images were 512×512 in size, with resolutions ranging from $0.299\,\text{mm} \times 0.299\,\text{mm}$ to $0.717\,\text{mm} \times 0.717\,\text{mm}$. The number of slices varied from 91 to 419, with thicknesses ranging from 0.330 mm to 1.0 mm. The ground truth was obtained through semi-automatic segmentation and manual repair by experienced clinicians. To focus on the orbital area, CT scans were resampled to 160×160 with a multiple of 32 slices after cutting out both orbits. This resulted in 240 single-orbital CT data for normal orbital segmentation training and 100 for OBF reconstruction training. The proposed networks used patches of size $32 \times 160 \times 160$, with training data augmented using sagittal symmetry.

The proposed and comparison networks all adopted the same input patch size of $32 \times 160 \times 160$, a batch size of 1, a learning rate of 0.001, and were trained for 30,000 iterations using TensorFlow 1.14 on an NVIDIA RTX 8000 GPU. Evaluation of the reconstruction results was based on the dice similarity coefficient (DSC), intersection over union (IOU), precision, sensitivity, average surface distance (ASD), and 95% Hausdorff distance (95HD).

Table 1. Evaluation results from ablation experiments of our method.

Networks	DSC (%) ↑	IOU (%) ↑	Precision (%) ↑	Sensitivity (%) ↑	ASD (mm) ↓	95HD (mm) ↓
SPAK	71.27 ± 4.28	55.53 ± 5.06	74.97 ± 4.98	68.02 ± 4.55	0.50 ± 0.08	1.80 ± 0.30
GN	87.97 ± 4.08	78.75 ± 6.14	89.40 ± 3.23	86.73 ± 5.74	0.20 ± 0.11	1.06 ± 0.59
GN+DN(GAN)	88.98 ± 3.15	80.28 ± 4.95	87.69 ± 3.95	90.41 ± 3.55	0.18 ± 0.09	0.96 ± 0.62
GN+ SPAK	91.87 ± 2.25	85.03 ± 3.75	$\mathbf{92.26 \pm 2.65}$	91.57 ± 3.30	0.12 ± 0.05	0.64 ± 0.26
Our method	$\mathbf{92.35 \pm 2.13}$	$\mathbf{85.86 \pm 3.53}$	92.01 ± 2.58	$\mathbf{92.75 \pm 2.66}$	$\mathbf{0.11 \pm 0.05}$	$\mathbf{0.59 \pm 0.23}$

3.2 Ablation Experiment Results

The proposed network is based on the GN, and an ablation experiment was conducted to verify the effectiveness of the adopted strategy. The experimental results are presented in Table 1. Comparing SPAK with other networks, it is evident that the accuracy of the reconstructed orbital wall is relatively poor, and it cannot be directly employed as a reconstruction network. However, it can be used as a prior guide for GAN. By comparing GN with GN+DN (GAN), it is apparent that the accuracy of GAN, except for precision, is better than GN. This finding shows that DN can promote GN to better reconstruct the orbital wall, indicating the correctness of adopting GAN as a reconstruction network for OBF. Furthermore, the addition of SPAK to GN and GAN significantly improved their reconstruction accuracy. Notably, compared with GAN, the proposed reconstruction network improved the DSC of orbital wall reconstruction accuracy by more than 3.5%, increased IOU by more than 5%, and decreased 95HD by 0.35 mm. These results indicate that SPAK guidance plays a crucial role in orbital wall reconstruction. It further demonstrates that the improved strategy can effectively achieve the precise reconstruction of the orbital wall in OBF.

3.3 Comparative Experiment Results

To demonstrate the superior performance of the proposed reconstruction algorithm, we compared it with several state-of-the-art networks used in medical image processing, including U-Net [15], V-Net [16], Attention U-Net [17], and Attention V-Net. The accuracy of the reconstructed results from these networks is compared in Table 2. The comparison with U-Net, V-Net, and Attention U-Net reveals that the proposed reconstruction network outperforms them significantly in terms of reconstruction accuracy evaluation. Specifically, the DSC is improved

Table 2. Evaluation results from ablation experiments of our method. Att U-Net denotes Attention U-Net, and Att V-Ne denotes Attention V-Net.

Networks	DSC (%) ↑	IOU (%) ↑	Precision (%) ↑	Sensitivity (%) ↑	ASD (mm) ↓	95HD (mm) ↓
U-Net [15]	88.01 ± 3.19	78.73 ± 5.02	88.27 ± 3.39	87.97 ± 5.23	0.20 ± 0.10	1.15 ± 0.10
V-Net [16]	89.42 ± 2.72	80.97 ± 4.39	91.04 ± 3.22	87.97 ± 3.65	0.18 ± 0.12	1.16 ± 1.78
Att U-Net [17]	87.46 ± 3.58	77.88 ± 5.37	91.05 ± 3.98	84.43 ± 5.95	0.22 ± 0.19	1.41 ± 2.50
Att V-Net	89.27 ± 8.81	80.77 ± 12.30	$\mathbf{92.11 \pm 12.50}$	86.71 ± 5.88	0.19 ± 0.19	0.90 ± 0.80
Our method	$\mathbf{92.35 \pm 2.13}$	$\mathbf{85.86 \pm 3.53}$	92.01 ± 2.58	$\mathbf{92.75 \pm 2.66}$	$\mathbf{0.11 \pm 0.05}$	$\mathbf{0.59 \pm 0.23}$

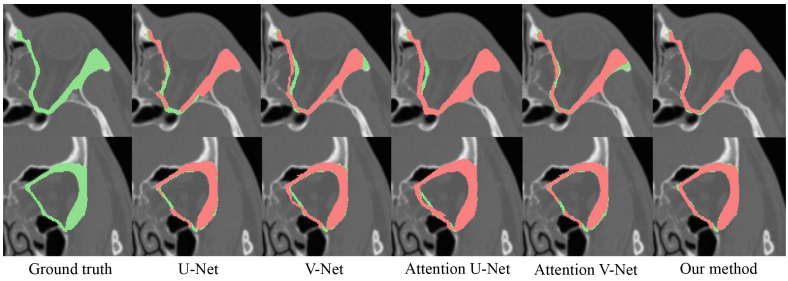

Fig. 3. Orbital wall reconstruction results comparisons between our network and other networks. Green is the ground truth, and red is the network's reconstruction result. (Color figure online)

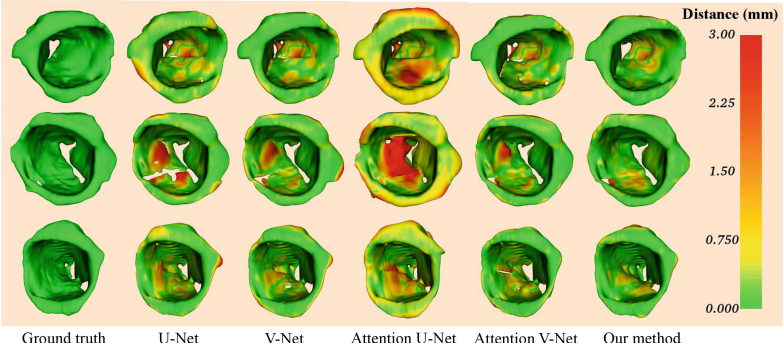

Fig. 4. Surface distance error comparisons between our network and other networks.

by more than 2.5%, the IOU is improved by more than 4.5%, the sensitivity is improved by more than 6.5%, and the 95HD distance error is reduced by more than 0.35 mm. These results indicate that the proposed network has better reconstruction performance for the orbital wall. Comparing with Attention V-Net, it is shown that the proposed reconstruction network has better reconstruction accuracy, except for precision. Although Attention V-Net has higher precision, its standard deviation is relatively large. Figure 3 is a comparison chart of the reconstruction results of each method, showing that other methods are difficult

to accurately predict the orbital wall boundary, while the proposed method can generate the orbital wall more accurately. Figure 4 presents a comparison chart of surface distance errors from the reconstruction results, which shows that other methods have relatively large distance errors in the medial and floor walls of the orbit, and even lead to cracks and holes. In contrast, the proposed network significantly addresses these issues, indicating its superior performance.

4 Conclusion

In summary, this paper proposes a SPAK-guided GAN for accurately automating OBF wall reconstruction. Firstly, we propose an automatic generation method of SPAK based on spatial transformation, which maps the segmented symmetrical normal orbital wall to a fractured orbit to form an effective SPAK. On this basis, a SPAK-guided GAN network is developed for the automatic reconstruction of the fractured orbital wall through adversarial learning. Furthermore, we use the strategy of multi-loss function supervision to improve the accuracy of network reconstruction. The final experimental results demonstrate that the proposed reconstruction network achieves accurate automatic reconstruction of the fractured orbital wall, with a DSC of $92.35 \pm 2.13\%$ and a 95% Hausdorff distance of 0.59 ± 0.23 mm, which is significantly better than other networks. This network achieves the automatic reconstruction of the orbital wall in OBF, which effectively improves the accuracy and efficiency of OBF surgical planning. In the future, it will have excellent application prospects in the repair surgery of OBF.

Acknowledgements. This work was supported by grants from the National Natural Science Foundation of China (81971709; M-0019; 82011530141), the China Postdoctoral Science Foundation (2023M732245), the Foundation of Science and Technology Commission of Shanghai Municipality (20490740700; 22Y11 911700), Shanghai Jiao Tong University Foundation on Medical and Technological Joint Science Research (YG2021ZD21; YG2021QN72; YG2022QN056; YG2023ZD19; YG2023ZD15), the Funding of Xiamen Science and Technology Bureau (No. 3502Z20221012), Cross disciplinary Research Fund of Shanghai Ninth People's Hospital, Shanghai Jiao Tong University School of Medicine (JYJC202115).

References

1. Ho, T.Q., Jupiter, D., Tsai, J.H., Czerwinski, M.: The incidence of ocular injuries in isolated orbital fractures. Ann. Plastic Surg. **78**(1), 59–61 (2017)
2. Rossin, E.J., Szypko, C., Giese, I., Hall, N., Gardiner, M.F., Lorch, A.: Factors associated with increased risk of serious ocular injury in the setting of orbital fracture. JAMA Ophthalmol. **139**(1), 77–83 (2021)
3. Ozturker, C., Sari, Y., Ozbilen, K.T., Ceylan, N.A., Tuncer, S.: Surgical repair of orbital blow-out fractures: outcomes and complications. Beyoglu Eye J. **7**(03), 199–206 (2022)
4. Xu, J., Zhang, D., Wang, C., Zhou, H., Li, Y., Chen, X.: Automatic segmentation of orbital wall from CT images via a thin wall region supervision-based multi-scale feature search network. Int. J. Comput. Assist. Radiol. Surg. 1–12 (2023)

5. Kim, H., et al.: Three-dimensional orbital wall modeling using paranasal sinus segmentation. J. Cranio-Maxillofacial Surg. **47**(6), 959–967 (2019)
6. Lee, M.J., Hong, H., Shim, K.W., Park, S.: MGB-net: orbital bone segmentation from head and neck CT images using multi-graylevel-bone convolutional networks. In: 2019 IEEE 16th International Symposium on Biomedical Imaging (ISBI 2019), pp. 692–695. IEEE (2019)
7. Taghizadeh, E., Terrier, A., Becce, F., Farron, A., Büchler, P.: Automated CT bone segmentation using statistical shape modelling and local template matching. Comput. Methods Biomech. Biomed. Eng. **22**(16), 1303–1310 (2019)
8. Li, J., et al.: Automatic skull defect restoration and cranial implant generation for cranioplasty. Med. Image Anal. **73**, 102171 (2021)
9. Xiao, D., et al.: Estimating reference shape model for personalized surgical reconstruction of craniomaxillofacial defects. IEEE Trans. Biomed. Eng. **68**(2), 362–373 (2020)
10. Han, B., et al.: Statistical and individual characteristics-based reconstruction for craniomaxillofacial surgery. Int. J. Comput. Assist. Radiol. Surg. **17**(6), 1155–1165 (2022)
11. Xu, J., et al.: A review on AI-based medical image computing in head and neck surgery. Phys. Med. Biol. (2022)
12. Nijiati, M., et al.: A symmetric prior knowledge based deep learning model for intracerebral hemorrhage lesion segmentation. Front. Physiol. **13**, 2481 (2022)
13. Guo, F., Ng, M., Kuling, G., Wright, G.: Cardiac MRI segmentation with sparse annotations: ensembling deep learning uncertainty and shape priors. Med. Image Anal. **81**, 102532 (2022)
14. Yuxin, W., He, K.: Group normalization. Int. J. Comput. Vision **128**(3), 742–755 (2020)
15. Ronneberger, O., Fischer, P., Brox, T.: U-net: convolutional networks for biomedical image segmentation. In: Navab, N., Hornegger, J., Wells, W.M., Frangi, A.F. (eds.) MICCAI 2015. LNCS, vol. 9351, pp. 234–241. Springer, Cham (2015). https://doi.org/10.1007/978-3-319-24574-4_28
16. Milletari, F., Navab, N., Ahmadi, S.-A., V-net: fully convolutional neural networks for volumetric medical image segmentation. In: 2016 fourth International Conference on 3D Vision (3DV), pp. 565–571. IEEE (2016)
17. Schlemper, J., et al.: Attention gated networks: learning to leverage salient regions in medical images. Med. Image Anal. **53**, 197–207 (2019)